JCI insight

TNFRSF13B genotypes control immune-mediated pathology by regulating the functions of innate B cells

Mayara Garcia de Mattos Barbosa, … , Jeffrey L. Platt, Marilia Cascalho

JCI Insight. 2021. https://doi.org/10.1172/jci.insight.150483.

Research In-Press Preview Genetics Inflammation

Graphical abstract

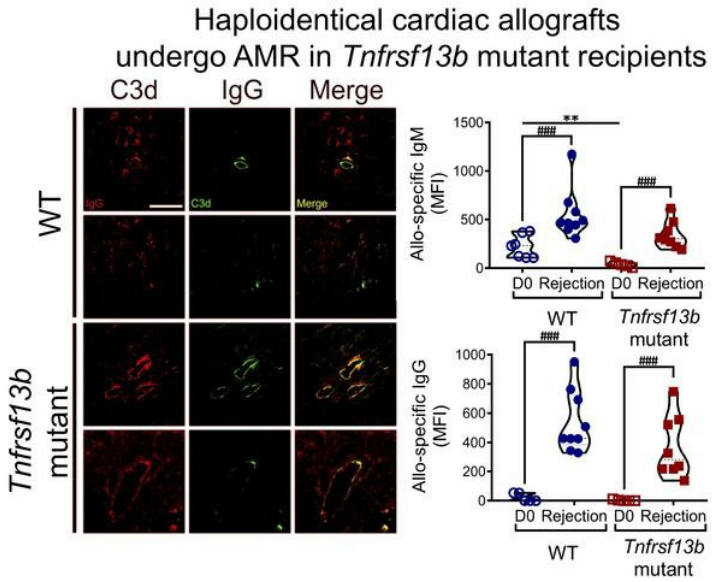

Find the latest version:

https://jci.me/150483/pdf

Title: ***TNFRSF13B*** **genotypes control immune-mediated pathology by regulating the functions of innate B cells**

Authors: Mayara Garcia de Mattos Barbosa[1], Adam R. Lefferts[1], Daniel Huynh[1], Hui Liu[1], Yu Zhang[1], Beverly Fu[1], Jenna Barnes[2], Milagros Samaniego[3], Richard J. Bram[4], Raif S. Geha[5], Ariella Shikanov[6], Eline T. Luning Prak[7], Evan Farkash[2], Jeffrey L. Platt[1,8,*], Marilia Cascalho[1,8,*]

[1]Department of Surgery, University of Michigan, Ann Arbor, MI, 48109, USA

[2]Department of Pathology, University of Michigan, Ann Arbor, MI, 48109, USA

3Department of Medicine, University of Michigan, Ann Arbor, MI, 48109, USA

[4]Department of Pediatric and Adolescent Medicine and Department of Immunology; Mayo Foundation; Rochester, MN, 55905, USA

[5]Division of Immunology, Boston Children's Hospital and Department of Pediatrics; Harvard Medical School; Boston, MA, 02115, USA

[6]Department of Biomedical Engineering; University of Michigan; Ann Arbor, MI, 48109, USA

[7]Department of Pathology and Laboratory Medicine; Perelman School of Medicine; University of Pennsylvania; Philadelphia, PA, 19104, USA

[8]Department of Microbiology and Immunology; University of Michigan; Ann Arbor, MI, 48109, USA

*Correspondence:

Marilia Cascalho

Address: Medical Science Research Building I, A520B

1150 West Medical Center Drive

Ann Arbor, Michigan 48109-5656

Phone: +1 (734) 615-6817

E-mail: marilia@med.umich.edu

Jeffrey L. Platt

Address: Medical Science Research Building I, A510E

1150 West Medical Center Drive

Ann Arbor, Michigan 48109-5656

Phone: +1 (734) 615-7755

E-mail: plattjl@med.umich.edu

Conflict of Interest Statement: The authors have declared that no conflict of interest exists.

Abstract:

Host genes define the severity of inflammation and immunity but specific loci doing so are unknown. Here we show that *TNFRSF13B* variants which enhance defense against certain pathogens, also control immune-mediated injury of transplants, by regulating innate B cells' functions. Analysis of *TNFRSF13B* in human kidney transplant recipients revealed that 33% of the subjects with antibody-mediated rejection (AMR) but less than 6% of those with stable graft function had *TNFRSF13B* missense mutations. To explore mechanisms underlying aggressive immune responses we investigated allo-immunity and rejection in mice. Cardiac allografts in *Tnfrsf13b*-mutant mice underwent early and severe AMR. The dominance and precocity of AMR in *Tnfrsf13b*-deficient mice was not caused by increased alloantibodies. Rather, *Tnfrsf13b* mutations decreased "natural" IgM and compromised complement regulation leading to complement deposition in allografted hearts and autogenous kidneys. Thus, wild type *TNFRSF13B* and *Tnfrsf13b* support innate B cell functions that limit complement-associated inflammation; in contrast, common variants of these genes, intensify inflammatory responses that help clear microbial infections but allow inadvertent tissue injury to ensue. The wide variation in inflammatory reactions associated with *TNFRSF13B* diversity suggests polymorphisms could underlie variation in host defense and explosive inflammatory responses that sometimes enhances morbidity associated with immune responses.

Main Text:

Introduction

Immunity and tolerance are governed at least in part by highly polymorphic genes of the MHC (1, 2), first appreciated as inherited determinants of the ability to produce antibodies against and reject foreign cells and tissues (3, 4). Yet, decades of experience in clinical transplantation reveals an inexact relationship between production of antibodies to foreign MHC and antibody-mediated rejection (AMR) of transplants expressing that MHC (5, 6). MHC also governs the ability to mount antibody responses to pathogens, which promote resistance and immunity in some (7), but appear to promote "autoimmune" pathology and explosive inflammatory reactions in others (8). Having recently discovered that a highly polymorphic gene (*TNF receptor superfamily member 13B, TNFRSF13B*) remote from MHC determines the character of primary immunity to enteric pathogens and whether immunity confers protection (9), we wondered whether and how variants of that gene could explain the not uncommon dissociation between transplant immunity and rejection of transplants and more broadly whether polymorphism at this locus could explain profoundly divergent impact of immunity and inflammation.

There are theoretical reasons to think that the *TNFRSF13B* genotype might influence the character and outcome of immunity (10). *TNFRSF13B* is among the most polymorphic genes in humans and other mammalian species. *TNFRSF13B* variants appear to have been under positive selection (11-13); MHC variants, in contrast, appear to have been under moderate purifying pressure (14). The protein encoded by *TNFRSF13B*, the "transmembrane activator calcium modulator and cyclophilin ligand interactor" (TACI), governs T cell-independent antibody

responses (15) and the maturation of and selection of T cell-dependent B cell responses (9). *TNFRSF13B* could thus govern the balance between immunity and tolerance (16).

To examine whether *TNFRSF13B* polymorphisms could weigh on immune-mediated pathology, we asked whether missense mutations in human subjects segregate with the antibody-mediated injury in kidney transplants and whether and how similarly disruptive genotypes in mice predispose to antibody-mediated injury in allografts. Our findings both in human and mouse reveal a clear association between *TNFRSF13B* genotype and the propensity of antibody responses to trigger allo-immune pathology. While this association might reflect several functions of *TNFRSF13B,* we show in mouse the propensity is owed to the functions of innate B cells. That the extraordinary polymorphism of *TNFRSF13B* has been maintained across mammalian species likely suggests the aggressive, highly inflammatory responses confer host defense; however, our results also show this benefit is balanced by the risk that immunity will eventuate in unbridled inflammatory reactions severe enough to destroy an organ. Understanding the phenotypes accompanying *TNFRSF13B* alleles might thus offer new insight into the genetic basis of host defense and disease.

Results

TNFRSF13B missense mutations in human kidney transplant recipients

Organ allografts commonly evoke B cell responses leading to production of alloantibodies. Depending on the sensitivity of the assay used, alloantibodies are detected at one time or another in about half of kidney transplant recipients (17, 18). Despite the frequent detection of alloantibodies, <20% of those with such antibodies develop acute AMR and occurrence is not

necessarily related to the level or the isotype of alloantibodies (18-20). We reasoned that if functions imparted by *TNFRSF13B* were of consequence for the biological impact of antibody responses, the frequency of *TNFRSF13B* missense mutations might differ in transplant recipients with AMR and recipients free of rejection.

To examine that possibility, we sequenced by the Sanger method the five exons of *TNFRSF13B* in a cohort of human kidney transplant recipients that developed AMR (exon 1, n=78; exon 2, n=67; exon 3, n=128; exon 4, n=167; exon 5, n=99) and in a cohort with stable graft function for up to five years after transplantation (exon 1, n=84; exon 2, n=110; exon 3, n=119; exon 4, n=115; exon 5, n=102) (Table 1). We did not find any missense mutations on *TNFRSF13B* exons 1 and 2 in either group. Several non-synonymous substitutions in exons 3, 4 and 5 are thought to perturb the TACI receptor function (11, 13, 21). More than 33% of those who developed AMR had missense mutations in exons 3 (C104R), 4 (A173T, A181E, K188del, K188M, G190R, S209F) and 5 (P251L), but less than 6% of the patients with stable graft function had these mutations ($p<0.0001$). Eight missense mutations (including one in frame deletion) in exons 3 and 4 were only present in kidney recipients who developed AMR. Only individuals with AMR had biallelic missense P251L mutations in exon 5 and included a compound heterozygote with two missense mutations on exon 4, A173T and K188M. Table 1 depicts the allele frequency of missense mutations in AMR and in stable graft function.

A summary of the expected impact of the variants on the function of the TACI receptor and in human health can be found summarized on Table S1 (22-26). These results suggest *TNFRSF13B* genotype might distinguish those who mount aggressive immunity to transplantation from those who do not; however, the degree of *TNFRSF13B* polymorphism in randomly bred populations and the many other potential variables would make it difficult to precisely connect a specific genotype

with an outcome, much less with underlying mechanisms. We therefore explored the potential impact of *Tnfrsf13b* on the aggressiveness of immune responses in inbred mice.

Tnfrsf13b and the rejection of organ transplants in mice

To determine whether and how the *Tnfrsf13b* genotype could influence the level and/or aggressiveness of antigen-specific antibody responses, we compared the outcome of organ transplants placed in wild type mice with the outcome in *Tnfrsf13b*-deficient mice. Hearts isolated from C57BL/6-BALB/c F1 (CB6F1) mice and transplanted heterotopically into C57BL/6 *Tnfrsf13b* wild type (WT) mice contracted for 13-39 days (average = 21.2 days) whereas hearts transplanted in *Tnfrsf13b*-deficient mice contracted for 7-21 days (average = 15.9 days; p=0.0136) (Figure 1A and Table 2). The most striking difference was not however in the length of graft function but instead the pathophysiology of allograft rejection. As expected, cardiac allografts in WT mice exhibited characteristic features of cell mediated rejection suggested by the accumulation of CD4- and CD8-positive T cells in the graft and no deposits of IgM, IgG or complement at 14 days post-transplantation (Figures 1B and S1). In contrast, the cardiac allografts in *Tnfrsf13b*-deficient mice contained abundant deposits of IgG and complement, features characteristic of AMR, as early as 14 days after transplantation (Figures 1B and S1). After 14 days features typical of cell-mediated rejection ensued in both *Tnfrsf13b*-deficient and WT recipients (Figures 1B and 1C). T cell infiltration appeared to increase as a function of time from transplantation (Figure 1D). Furthermore, grafts in mutant mice had significantly less T regulatory cells (T regs)/mm^2 than grafts in wild type recipients (Figures 1B and 1C). Consistent with a lack of impact on cellular immunity, skin allografts from CB6F1 were rejected as fast in *Tnfrsf13b-KO* as in WT recipients (Figure 1A and Table 2). Spontaneous AMR preceding cell-mediated lesions of organ transplants is quite

unusual unless the recipient was previously sensitized to allo-antigens or genetically manipulated in ways that profoundly increase production of alloantibodies (27). Since *Tnfrsf13b* deficiency decreases baseline production of antibodies and impairs maturation of B cell responses to antigen (28), the propensity toward development of AMR in *Tnfrsf13b*-deficient mice and possibly in humans with *TNFRSF13B* mutations would seem contrary to canonical functions of *TNFRSF13B*.

To determine whether disruption of *Tnfrsf13b* increases the magnitude of antibody response, accelerating rejection and causing dominance of antibody-mediated over cell-mediated pathology of allografts early in the graft's life, we assayed alloantibodies in allograft recipients before transplantation and at the time of rejection. As Figure 1E shows, both WT and *Tnfrsf13b*-deficient mice mounted appreciable alloantibody responses after cardiac allo-transplantation; however, the responses in *Tnfrsf13b*-deficient mice were less robust than responses in wild type mice (IgM, $p=0.018$; IgG, $p=0.057$). Thus, the amount of alloantibody detected after transplantation would not appear to explain the dominance of antibody-mediated pathology in mutant recipients. Because non-synonymous mutations in *TNFRSF13B* have been associated with autoantibodies which could contribute to disease of the transplanted heart we detected autoantibodies by staining the native hearts of both WT and *Tnfrsf13b*-deficient mice, also retrieved at rejection. Native hearts showed no deposition of IgM, IgG or complement indicating negligible autoantibody response in transplanted mice (Figure S2).

Organ allografts can absorb a substantial fraction of alloantibody from serum and hence it was possible that *Tnfrsf13b*-deficient mice produced more alloantibody than wild type mice, but the increase was obscured by absorption. To exclude that possibility, we injected allogeneic splenocytes and thymocytes into the peritoneal cavity of wild type and in *Tnfrsf13b*-deficient mice and assayed alloantibodies at various times thereafter. Because full *TNFRSF13B* deficiency is

rarely observed in humans (16), we also tested the impact of mono-allelic A144E missense mutations, which is homologous to a common human variant, A181E, that was detected in two transplant recipients with AMR (Table 1). As Figure 2 shows, mono-allelic, bi-allelic mutants and *Tnfrsf13b*-deficient mice produced no more IgG allo-antibodies and significantly less IgM allo-antibodies than wild type controls.

To confirm that *Tnfrsf13b*-mutant mice do not mount more robust allo-specific B cell responses, despite the propensity to inflict AMR on cardiac allografts, we enumerated the various types of B cells and the frequency of antibody-secreting cells in the spleens of wild type and mutant mice before and after exposure to allogeneic splenocytes and thymocytes (respectively Figures S3 and 3A). The immunized mutant mice had more total B cells and more B cells in marginal zones (MZ), follicles and germinal centers (GC) than wild type mice (Figure 3A), consistent with increased response to activation (9, 29). However, relatively few of these B cells secreted antibody (Figure 3B). Clearly, some *Tnfrsf13b* missense mutations can underlie more aggressive B cell effector responses, possibly at the cost of inadvertent pathogenicity; however, neither the amplitude nor the pathogenicity are simple functions of the amount of antigen-specific IgG produced.

Tnfrsf13b and the regulation of immunity

B cells exert functions besides production of antigen-specific IgG. Since IgG production was necessary but not sufficient to explain the dominance of the B cell effector responses in *Tnfrsf13b*-deficient or mutant mice (9), we wondered whether *Tnfrsf13b* governs processes besides production of IgG that could explain the differential aggressiveness of immune responses. To address that question, we surveyed gene expression in germinal center B cells isolated from the spleens of mice that had been immunized with allogeneic splenocytes and thymocytes (Figures S4, 4A and Table

S2). As expected, B cells from the germinal centers, in which IgG responses to allogeneic cells originate, of wild type mice exhibited more pronounced expression of Ig light and heavy chain genes (17 genes in WT *vs. Tnfrsf13b*-KO, p=0.0001; and 12/111 genes in WT *vs.* A144E/A144E, p=0.0028) and genes governing plasma cell differentiation (17/151 genes in WT *vs. Tnfrsf13b*-KO, p=0.002) than GC B cells from mutant mice (Figure 4B). This confirmed the idea that IgG production and B cell maturation do not underlie the aggressive and potentially injurious humoral responses in mice and humans. What could not be anticipated however was that GC B cells from immune wild type mice also exhibited greater expression of genes associated with immune regulation. Those included *Forkhead box P3* (*Foxp3*), *Indoleamine 2,3-dioxygenase 1* (*Ido1*), *Interleukin 10* (*Il10)* and genes associated with B regulatory cell functions such as *Cd9 antigen* (*Cd9*), *Cd5 antigen* (*Cd5*), *CD1d1 molecule* (*Cd1d1* and *Cd1d2*) and *Hepatitis A virus cellular receptor 1* (*Havcr1*), which encodes T cell Ig mucin-1 (Tim-1), among others (Figure 4B). It is possible these functions supported a modest prolongation of survival of cardiac allografts in several wild type mice and could have significance in clinical transplantation where B cells are implicated in immune regulation and tolerance (30). However, the fast development of antibody-mediated injury to transplants in mutant mice is unlikely the direct consequence of defective immune regulation alone since cellular immunity develops as fast in in WT as in mutant mice (Figures 1A-D). Accordingly, we questioned whether the aggressive effector responses in mutant mice could reflect deficiency of natural or more rapidly recruited controls of tissue injury, such as availability of natural antibodies (31).

C***ontrol of complement and tissue injury by natural and elicited antibodies***

Natural antibodies, so named because they are present without prior exposure to antigen, have been postulated to provide initial defense against pathogens, but also to promote repair of cellular injury

and control of inflammatory reactions and complement (31-34). We wondered whether a deficiency of natural antibodies might explain the severe manifestations of humoral immunity in *Tnfrsf13b*-mutant mice. *Tnfrsf13b*-deficient, and mono- and bi-allelic A144E-mutant mice were indeed deficient of IgM at baseline (Figures 2A, S5A and S5B) and after immunization with allogeneic cells (Figures 2A, 2B and S5A-C). The deficiency included the fraction of IgM that binds double-stranded DNA (dsDNA), single-stranded DNA (ssDNA), cardiolipin (CL), thyroglobulin (TG), lipopolysaccharide (LPS) and phosphocholine (PC), common targets of polyreactive natural antibodies (Figure 5). Thus, *Tnfrsf13b* controls the amount of IgM "natural" antibodies implicated in the control of inflammation and complement activation.

Natural antibodies, especially IgM, regulate complement by reacting with C3b before it can fix on eukaryotic cellular targets (31-33, 35). We therefore reasoned that if the aggressive humoral effector activity in *Tnfrsf13b*-deficient mice was owed to deficiency of complement-regulating IgM, excess C3b generated in allografts or by spontaneous alternative pathway tick over (36) would be available to fix to autologous (non-transplanted) tissues. To test that possibility, we examined native kidney tissues from un-manipulated mice and from mice immunized 8 days earlier with allogeneic cells. As Figure 6A shows, the kidneys of un-manipulated mutant mice contained appreciable deposits of C3d, and the deposits were increased with immunization. In contrast, the kidneys of un-manipulated and immunized wild type mice contained little or no deposits of C3d. Complement deposition was accompanied by IgM and IgG deposition indicating damage in the native kidney (Figure S6).

To test if deficiency of "natural" IgM alone (and not any other feature associated with TACI function) caused complement dysregulation we measured C3d deposits in the native kidneys in mice that lack "natural" antibodies, the quasi-monoclonal (QM) mouse (37, 38) expressing wild

type or *Tnfrsf13b*-KO alleles. The QM mouse produces mostly monoclonal IgM that recognizes a synthetic hapten and is not cross-reactive. Immunofluorescence staining of kidney sections obtained from naïve QM *Tnfrsf13b*-WT or QM *Tnfrsf13b*-KO mice show abundant deposition of C3d, and IgG (Figure S7A and S7B). In the absence of "natural" IgM, C3d deposition occurs independently of *Tnfrsf13b* expression and fully allogenic grafts (BALB/c; H-$2^{d/d}$) are rejected in QM recipients with kinetics comparable to rejection of allografts in C57BL/6 controls (Figure S7C). These results suggest that *Tnfrsf13b* promotes production of natural antibodies that regulate complement and possibly other elements of inflammation at baseline and during immune responses to avert incidental injury. In contrast, *Tnfrsf13b* mutations that commonly disrupt the function of the protein leave humoral immunity untethered, allowing increasing injury to foreign targets (and hence host defense) but potentially allowing incidental injury to other tissues and organs.

TNFRSF13B missense mutations in recipients of kidney transplants are associated with decreased C3 and natural antibodies in the blood

To glimpse the possibility that defective control of complement in *Tnfrsf13b*-mutant mice might also occur in humans, we measured LPS-binding IgM natural antibodies and C3 in the blood of kidney transplant recipients. As Figure 6B shows transplant recipients with *TNFRSF13B* missense mutations had significantly lower concentrations LPS-bound IgM natural antibodies as a fraction of IgM, and less C3 in serum than transplant recipients with two wild type alleles independently of transplant outcome. Reduced C3 levels and LPS-bound IgM in the blood after transplantation were also associated with AMR as compared to the group with good outcome (Figure 6C). These findings suggest that *TNFRSF13B* missense mutations decrease natural antibodies and increase C3 activation.

Discussion

Here we show that *TNFRSF13B* controls the character and aggressiveness of immune responses. In contrast to MHC, *TNFRSF13B* does not impact on the initiation of an immune response *per se* but rather on its regulation by virtue of controlling "natural" antibodies produced by innate B cells. Thus, by inhibiting natural antibody secretion (IgM and IgA) and favoring adaptive antibody responses, *TNFRSF13B* diversity establishes varying susceptibility to infection (9, 39), autoimmunity (40, 41), immunodeficiency (15, 21, 42-44) and excessive inflammatory reactions to transplantation and perhaps to pathogens as well.

The *TNFRSF13B*-deficiency heightened propensity for AMR, and particularly increased deposition of C3d, results from two related features of the mutant phenotype. First, *Tnfrsf13b* mutants have lower baseline levels of Ig and notable deficiency of IgM and IgA (29)(43), (produced by marginal zone B cells and peritoneal B1 cells); but mutants can still produce high affinity IgG (in germinal centers) (9). The high affinity IgG produced by mutant mice effectively prevents certain infections (9) and here we show it can initiate antibody-mediated rejection. But as important as production of high affinity IgG may be the second feature of the phenotype, the scarcity of IgM and IgA also contributes to rejection. All Ig, but especially IgM and IgA, can provide alternative substrate for fixation of C3b. If Ig binds weakly or not at all to a target, the fixation of C3b diverts this active moiety away from cell surfaces, effectively decreasing local complement fixation (36). Tightly bound Ig in contrast has the opposite effect, potentially increasing the amount of local complement activation. Thus, mutant mice have the ability to produce allo-specific antibodies but lack the regulatory activity conferred by unbound and weakly bound Ig.

The physiologic impact of some *TNFRSF13B* polymorphisms has been determined (45-47) and simultaneously manifest benefits and risks evidenced by balancing selection at this locus (12), but the relationship between many polymorphisms and specific phenotypes remains to be fully elucidated (10). *TNFRSF13B* genotypes that disrupt the function of the encoded protein favor highly aggressive humoral immune responses, the wild type allows both cell-mediated and antibody-mediated responses to proceed, albeit with restraint. Although we used immune responses to transplantation in mice and humans to explore the impact of disruptive genes on the phenotype (since every animal and human subject potentially mounts a biologically impactful response), it is not difficult to imagine how the range of phenotypes of *TNFRSF13B* variants would impact on host defense and disease. For example, *Tnfrsf13b*-mutant mice mount faster and more effective B cell responses than wild type mice to enteric pathogens that model enteropathogenic *E. coli* that causes widespread acute and chronic enteritis (9). We recently found that mutant strains with *Tnfrsf13b* haplo-insufficiency or deficiency (39) also delimit transmission (Platt *et al.*, accepted for publication), and that might explain the apparently positive selection of disabling variants (11-13). Yet, the wild type *TNFRSF13B* and *Tnfrsf13b* also have favorable characteristics. Not only does the wild type allow full maturation of B cell responses (28), we show here that the wild type also governs the extent of inflammation and activation of complement that occur at baseline and upon exposure to antigen by controlling the functions of innate B cells. The importance of control of inflammation and complement reactions has been recently highlighted by untoward responses in some infected with the SARS-CoV-2 virus (48, 49).

The profound diversity of *TNFRSF13B* and *Tnfrsf13b* across mammalian species (11) further supports the concept that phenotypes we describe in transplant recipients have broader biological significance. The limited analysis of *TNFRSF13B* sequences reveals as much diversity

as MHC and suggests that both the wild type and missense variants are sustained by positive selection even-though most individual SNPs are rare and do not perturb expression of the protein. (11-13). Although, the full extent of *TNFRSF13B* diversity and implications for physiology remain to be established (doing so will depend on meticulous sequencing of all exons and regulatory sequences), our results suggest the potential value. The need for full sequencing of polymorphic genes is highlighted by the failure genome-wide-association studies to identify *TNFRSF13B* SNPs as a risk factor for rejection (50-52).

In transplantation much effort has been devoted to identifying recipients at heightened risk of developing antibody-mediated rejection because this type of rejection poses the most significant risk for early demise of organ grafts. Sensitization to donor antigens poses such a risk that transplantation might be delayed or avoided entirely if it is detected. But, as most transplant recipients are not pre-sensitized, the risk of antibody-mediated disease is uncertain. Probing *TNFRSF13B* sequence and/or function might address that question and also help explain why some individuals with autoantibodies develop autoimmune disease while many with the same antibodies have no evident disease and, why some individuals mount destructive inflammatory responses following viral infections while others remain asymptomatic. Since the receptor encoded by *TNFRSF13B* is actionable by modified ligands and/or antibodies our discovery suggests a new avenue for anti-inflammatory therapeutics, either supplementing intermediates produced by *TNFRSF13B* or providing the appropriate end products for those lacking or with decreased *TNFRSF13B* function.

Methods

Human Participants

The experimental cohorts were drawn from the active and inactive patients in the transplant nephrology service at the University of Michigan. The cohorts were matched for donor variables (age, race, gender, height, weight, creatinine, diabetes, hypertension, cigarette use, Hepatitis C); transplant variables [pulsatile perfusion, cold ischemia time, organ sharing (local, regional, national), HLA mismatch score, year of transplant, enbloc/double, ABO compatibility] and for recipient variables [age, race, gender, diagnosis, pre-transplant blood transfusion, body mass index, peak panel reactive antibodies (PRA)/calculated PRA, pre-transplant years of dialysis, immune-suppressive therapy including use of T cell depletion agents, angina, peripheral vascular disease, drug-treated chronic obstructive pulmonary disease and Hepatitis C virus infection]. The patients were identified using the list of transplant recipients currently or previously followed at the University of Michigan or at the University of Wisconsin, curated by the Organ Transplantation Information System (OTIS) and in coordination with the honest broker's office. The presence or absence of rejection was defined based on decreased graft function and biopsy findings typical of antibody-mediated rejection. Diagnosis of antibody-mediated rejection is usually based on pathologic findings that include C4d deposition in peritubular capillaries or glomerular capillaries, peritubular or glomerular capillary inflammation, and glomerular basement membrane duplication. In the antibody-mediated rejection group we also included patients with donor-specific antibodies that were persistent, found in more than one occasion, even if there was no evidence of rejection on the biopsy. Protocol biopsies were examined for presence of C4d and/or glomerulitis and/or peritubular capillaritis (53). Stable graft function was defined as absence of an unexplained decrease in the estimated glomerular filtration rate (eGFR) >15% from baseline. Unexplained

decreases in the eGFR usually prompt a transplant biopsy and clinical testing of donor-specific antibodies. Individuals with proteinuria >500 mg were excluded to avoid uncertainties about etiology (i.e. transplant glomerulopathy, which rarely causes significant proteinuria in the first year, versus *de novo* or recurrent disease).

***TNFRSF13B* sequencing and analysis**

The *TNFRSF13B* gene is located on chromosome 17 and is composed of 5 exons spanning 34Kb. We amplified the exons 3 and 4 with the primers described by Salzer and colleagues (42). Exon 5 was amplified using 2 pairs of primers: 5' CTGCCCACACCGTCACCCCTACC 3' and 5' CTCTCCCCTCTCCCCACCTCTC 3', and 5' GGGGGTCAGGGAGGGAAAGGAG 3' and 5' TGATGCCCAGGAAAGTGATAGACAAG 3'. Genomic DNA was extracted from peripheral blood cells using DNeasy Blood & Tissue Kit following the manufacturer directions (Qiagen Cat#69504). Alternatively, DNA samples were obtained from the Michigan Genome Initiative (MGI). Polymerase chain reaction was performed with Taq DNA Polymerase, native (Thermo Fisher Scientific Cat#18038-042) at 95-15:00+45x(94-0:30+60-0:15+72-0:30)+72-1:00. Samples were run in a 2% agarose gel; specific bands were cut out and the DNA was purified with QIAquick Gel Extraction Kit (Qiagen Cat#28706). Sequences were obtained by Sanger sequencing performed at the University of Michigan Sequencing Core facility and aligned using Sequencher 5.4.6 software (Gene Codes Corporation, Ann Arbor, MI).

Mice

BALB/cJ (Cat#000651), CB6F1/J (Cat#100007) and C57BL/6J (Cat#000664) *Tnfrsf13b* wild type mice were purchased from The Jackson Laboratory. *Tnfrsf13b*-KO mice (54) and mice harboring bi-allelic (A144E/A144E) or mono-allelic A144E mutations (A144E/WT) (39), homologous to the

human A181E mutation, were previously described. QM mice have been described previously (37, 38) and were bred with *Tnfrsf13b*-KO mice to produce QM *Tnfrsf13b*-KO mice. All the *Tnfrsf13b*-mutatnt mice were bred onto the C57BL/6 background. Animal experimentation was performed in mice of both genders between 8-20 weeks of age.

Heart and Skin Allografts

Hearts from CB6F1 (C57BL/6-BALB/J F1, H-$2^{b/d}$ haplotype) mice were transplanted heterotopically into the abdomen of C57BL/6 background wild type and *Tnfrsf13b*-deficient mice (H-$2^{b/b}$ haplotype). Hybrid mice sharing a haplotype with the recipient were used as sources of grafts to minimize the impact of natural killer cells. Alternatively, hearts from BALB/c (H-$2^{d/d}$) were transplanted heterotopically into the abdomen of C57BL/6 background QM and QM *Tnfrsf13b*-deficient mice (H-$2^{b/b}$ haplotype). Heterotopic cardiac transplants do not confer cardiac function in the recipient because the heart muscle is perfused, but heart chambers are not connected to the circulation, but the grafts can undergo rejection as would an experimental or clinical transplant. The grafts were palpated daily, and rejection was considered when the hearts stopped beating. The mice were sacrificed on rejection day and the transplanted hearts, spleens and sera were collected. All the transplanted mice were maintained in the absence of immunosuppression. Skin grafts from CB6F1 were transplanted into C57BL/6 background wild type and *Tnfrsf13b*-deficient mice. The grafts were observed daily, and rejection was considered when 50% of the graft became necrotic. All the transplanted mice were maintained in the absence of immunosuppression.

Allogeneic Stimulation

Wild type, *Tnfrsf13b*-deficient, bi-allelic, and mono-allelic *Tnfrsf13b* A144E-mutant mice (H-$2^{b/b}$ haplotype) were immunized by intraperitoneal injection with 5 x 10^7 BALB/c splenocytes and

thymocytes (H-$2^{d/d}$ haplotype). After 8-21 days the mice were sacrificed and the sera, spleens and kidneys were collected for posterior analysis. Alternatively, non-immunized mice were used as control.

Flow Cytometry and Antibodies

Splenocytes and peritoneal cells were isolated from mice immunized with allogeneic cells, transplanted or naïve mice, counted and frozen for posterior analysis. The cell viability was assessed by staining with BD Horizon Fixable Viability Stain 780 (FVS780; 1.11 µg/mL; BD Biosciences Cat#565388). Splenocytes were stained with FITC-conjugated antibodies rat anti-mouse CD19 (1D3; 10 µg/mL; BD Biosciences Cat# 553785, RRID:AB_395049), CD23 (B3B4; 10 µg/mL; BD Biosciences Cat#553138, RRID:AB_394653) or Armenian hamster anti-mouse CD95 (Jo2; 10 µg/mL; BD Biosciences Cat#554257, RRID:AB_395329); PE-conjugated rat anti-mouse CD19 (1D3; 4 µg/mL; BD Biosciences Cat#557399, RRID:AB_396682), GL7 (GL7; 4 µg/mL; BD Biosciences Cat#561530, RRID:AB_10715834) or IgD (11-26c.2a; 4 µg/mL; BD Biosciences Cat#558597, RRID:AB_647211); PerCP-Cy5.5-conjugated rat anti-mouse CD21/CD35 (7G6; 4 µg/mL; BD Biosciences Cat#562797, RRID:AB_2737802); APC-conjugated rat anti-mouse B220 (RA3-6B2; 4 µg/mL; Thermo Fisher Scientific Cat#17-0452-81, RRID:AB_469394) or CD19 (1D3; 4 µg/mL; BD Biosciences Cat#550992, RRID:AB_39848). Multiparametric flow cytometric analysis of 10^6 stained cells was performed using a BD FACSCanto II (BD Biosciences, Franklin Lakes, NJ) and 100,000 events were analyzed with FlowJo 10 software (FlowJo, LLC, Ashland, OR, RRID:SCR_008520). In addition, splenocytes and peritoneal from mice immunized with allogeneic cells for 10 days were stained with, respectively, FVS780, anti-CD19 APC, GL7 PE and CD95 FITC, and FVS780, anti-CD19 PerCP-Cy5.5, CD23 PE-Cy7, IgM Alexa Fluor 488 and IgD PE as described above and germinal center

(GC) B cells ($FVS780^{-}$ $CD19^{+}$ $GL7^{+}$ $CD95^{+}$) (Figure S4A) were sorted in a Synergy SY3200 Cell Sorter (Sony Biotechnology, San Jose, CA, USA) at the University of Michigan Flow Cytometry Core.

RNA Extraction and Gene Expression Analysis of Germinal Center B cells

The RNA from the sorted GC B cells was extracted with the RNeasy Plus Mini Kit (Qiagen Cat#74134) as recommended by the manufacturer. Next, the RNA integrity (RIN) and amount was analyzed by RNA quality control (QC) analysis using Agilent RNA 6000 Pico Kit (Agilent Technologies Cat#5067-1513) in an Agilent 2100 Bioanalyzer (Agilent Technologies, Santa Clara, CA). All the samples used for the microarray analysis had RIN values between 8.8 and 10. The gene expression was assessed using a GeneChip Mouse Gene 2.1 ST Array Plate (Affymetrix Cat#902140). The distribution of the probes for each chip was analyzed and the standard error for each gene on each array was assessed after fitting a probe-level model (Figure S4B). Expression values for each gene were calculated using a robust multi-array average (55) and transformed in log_2 values. Values were fit in a principal component analysis (PCA) and the first two principal components were plotted to show sample gene expression clusters (Figure S4C). Data were fit to weighted linear models (56) and the contrasts of interest were computed. Additionally, the expression data were also weighted in a gene-by- gene update algorithm designed to downweight chips that are deemed less reproducible (57). The probesets with a fold change greater than 2 were selected and the p values were adjusted for multiple comparison using false discovery rate (58). A p value equal or less than 0.05 was deemed significant. All analyzes were performed using oligo and limma packages of biocondutor implemented in the R statistical environment (R version 3.4.3). Additionally, the gene expression data were loaded into iPathwayGuide software (Advaita

Bioinformatics, Plymouth, MI), volcano plots were generated (Figure S4D) and cellular process pathways were analyzed.

Enzyme-Linked ImmunoSpot for Detection of Immunoglobulin-Secreting Cells

96-well Filtration Plate MultiScreen HTS HA Sterile Plates (MilliPore Cat#MSHAS4510) were activated and coated for 1 hour at room temperature with goat anti-mouse Ig (H+L) (4 µg/mL; SouthernBiotech Cat#1010-01, RRID:AB_2794121). After blocking overnight at 4° C, mouse splenocytes or peritoneal cells were platted in serial dilutions, starting with 10^5 cells per well, and incubated at 37° C in 5% CO_2 atmosphere overnight. Spots of bound IgG or IgM were detected by adding the alkaline phosphatase-conjugated antibodies goat anti-mouse IgG (0.5 µg/mL; SouthernBiotech Cat#1030-04, RRID:AB_2794293) or goat anti-mouse IgM (0.5 µg/mL; SouthernBiotech Cat#1020-04, RRID:AB_2794200) for 1 hour at room temperature. The reaction was visualized by subsequent addition of 5-bromo-4-chloro-3-indolylphosphate/nitro blue tetrazolium substrate (Sigma-Aldrich Cat#B5655-5TAB). The number of spots was assed via a CTL ImmunoSpot S5 UV Analyzer equipped with ImmunoSpot ImmunoCapture and ImmunoSpot Counting softwares (Cellular Technology Ltd., Cleveland, OH, RRID:SCR_011082).

Enzyme-Linked Immunosorbent Assay for Detection of Mouse Immunoglobulins

Nunc MaxiSorp ELISA plates (Thermo Fisher Scientific Cat# 44-2404-21) were coated overnight with goat anti-mouse Ig (H+L) (4 µg/mL; SouthernBiotech Cat#1010-01, RRID:AB_2794121). After blocking, the plates were incubated with transplanted or allogeneic-stimulated mice serum. Bound IgG or IgM were detected by adding goat anti-mouse IgG-HRP (4 µg/mL; SouthernBiotech Cat#1030-05, RRID:AB_2619742) or goat anti-mouse IgM-HRP (4 µg/mL; SouthernBiotech Cat#1020-05, RRID:AB_2794201). Alternatively, polyreactive natural IgM was detected by

analyzing the amount of immunoglobulin bound to lipopolysaccharide (LPS), thyroglobulin (TG), cardiolipin (CL), double-stranded DNA (dsDNA), single-stranded DNA (ssDNA) and phosphocholine (PC) adapted from the protocol described by Singh et al. (59). Briefly, Nunc MaxiSorp ELISA plates were coated overnight at room temperature with TG (10 µg/mL; Alpha Diagnostic International Cat#THGL15-N-1), CL (10 µg/mL; Sigma Cat#C0563-10MG), LPS (10 µg/mL; Alpha Diagnostic International Cat#LPS12-1), dsDNA, ssDNA (10 µg/mL; Sigma Cat#D8515-1G) or PC (10 µg/mL; Sigma Cat#P0378). After blocking, mice sera were incubated for 2 hours at 37° C. Bound IgM was detected by adding goat anti-mouse IgM-HRP (4 µg/mL; SouthernBiotech Cat#1020-05; RRID:AB_2794201). The reactions were visualized by subsequent addition of 2,2′-Azino-bis (3-ethylbenzthiazoline-6-sulfonic acid) substrate (SouthernBiotech Cat#0202-01). All readings were recorded at 405 nm.

Allo-Specific Antibodies Detection by Flow Cytometry

Titers of allo-specific IgG and IgM in the sera before and after the heart transplant rejection and at different times after the immunization with allogeneic cells were assessed by flow cytometry. Briefly, BALB/c thymocytes (allogeneic) were incubated with different concentrations of serum for 30 minutes at 4° C. The thymocytes were washed and bound antibodies were detected with Cy5-conjugated goat anti-mouse IgG (4 µg/mL, SouthernBiotech Cat#1030-15, RRID:AB_2794299) or Alexa Fluor 488-conjugated goat anti-mouse IgM (4 µg/mL, SouthernBiotech Cat#1020-30, RRID:AB_2794219) for 30 minutes at 4° C and analyzed in a BD FACSCanto II (BD Biosciences, Franklin Lakes, NJ). The mean fluorescence intensities (MFI) in the APC-channel (measuring bound IgG) and FITC channel (measuring bound IgM) were determined with FlowJo 10 software (FlowJo, LLC, Ashland, OR, RRID:SCR_008520) inside the lymphocyte gate.

Histopathology and Immunofluorescence

Upon sacrifice, the transplanted hearts were sectioned, and part was fixed, embedded in paraffin and stained with Hematoxylin and Eosin (H&E) to perform the histological studies. Alternatively, sections of the transplanted heart and naïve and immunized mice kidneys were snap frozen in Tissue-Tek Optimal Cutting Temperature (O.C.T.) Compound (Sakura Finetek Cat# 4583) and snap frozen. Five microns cryosections were processed and the native and transplanted heart sections were incubated with the primary antibodies goat anti–mouse C3d (800 ng/mL, R and D Systems Cat#AF2655, RRID:AB_2066622), goat anti-mouse IgM, human ads (10 µg/mL; Southern Biotech Cat#1020-01, RRID:AB_2794197) for 1 hour at 4° C, followed by CF555-conjugated donkey anti–goat IgG (20 µg/mL; Sigma-Aldrich Cat#SAB4600059-250UL) or Alexa Fluor Plus 488-conjugated donkey anti–goat IgG (4 µg/mL; Thermo Fisher Scientific Cat# A32814, RRID:AB_2762838); rat anti–mouse CD4 (GK1.5) (10 µg/mL; eBioscience Cat#14-0041-86, RRID:AB_467065) or rat anti-mouse CD8a (53-6.7) (10 µg/mL; BD Biosciences Cat#553027, RRID:AB_394565) for 1 hour at 4° C, followed by CF488-conjugated goat anti-rat IgG (20 µg/mL; Sigma-Aldrich Cat#SAB4600046-250UL); rabbit anti-mouse FoxP3 (2 µg/mL; Novus Biologicals Cat#NB100-39002SS, RRID:AB_1290944) for 1 hour at 4° C, followed by CF555-conjugated goat anti-rabbit IgG (20 µg/mL; Sigma-Aldrich Cat#SAB4600068-250UL, RRID:AB_2336059); or Texas Red-X-conjugated goat anti-mouse IgG (8 µg/mL; Thermo Fisher Scientific Cat#T-862, RRID:AB_2556781) incubated for 1 hour at 4° C. Additionally, native kidneys from naïve and mice immunized with allogeneic cells were stained with anti-IgM, anti-IgG and anti-C3d as described above. For contrast, nuclei were stained with DAPI and slides were mounted with anti-fade mounting media. The slides were examined with a Leica DMI6000B microscope equipped with a Leica DFC360 FX monochrome digital camera and a Leica HCX PL FLUOTAR L 40X/0.60

CORR PH2 microscope objective (Leica Microsystems, Wetzlar, Germany). At least 5 fields were imaged at 400x magnification via QCapture Pro 7 software (QImaging, Surrey, Canada, RRID:SCR_014432). For the native kidney slides, the glomeruli area was selected with aid of the tissue green auto-fluorescence and the differential interference contrast (DIC) in stacked images and the mean fluorescence intensity (MFI) of IgM, IgG or C3d in the selected area was assed via Adobe Photoshop CC software (Adobe Systems Incorporated, San Jose, CA, RRID:SCR_014199).

Enzyme-Linked Immunosorbent Assay for Detection of Human Immunoglobulins

Nunc MaxiSorp ELISA plates (Thermo Fisher Scientific Cat# 44-2404-21) were coated overnight with goat anti-human IgM (4 µg/mL; SouthernBiotech Cat#2020-01, RRID:AB_2795599). After blocking, the plates were incubated with serum from transplanted patients. Bound IgM was detected by adding HRP-conjugated goat anti-human IgM (4 µg/mL; SouthernBiotech Cat#2020-05, RRID:AB_2795603). Alternatively, polyreactive natural IgM was detected by analyzing the amount of immunoglobulin bound to lipopolysaccharide (LPS) adapted from the protocol described by Singh et al. (59). Briefly, Nunc MaxiSorp ELISA plates were coated overnight at room temperature with LPS (10 µg/mL; Alpha Diagnostic International Cat#LPS12-1). After blocking, human sera were incubated for 2 hours at 37° C. Bound IgM was detected by adding goat anti-human IgM-HRP (4 µg/mL; SouthernBiotech Cat#2020-05, RRID:AB_2795603). The reactions were visualized by subsequent addition of 2,2′-Azino-bis (3-ethylbenzthiazoline-6-sulfonic acid) substrate (SouthernBiotech Cat#0202-01). All readings were recorded at 405 nm.

Enzyme-Linked Immunosorbent Assay for Detection of Human C3

The concentration of complement component 3 in the serum of the kidney transplant recipients was assessed with the Human Complement C3 ELISA Kit (Abcam Cat#ab108822) according to the manufacturer's instructions. Reference values: 800 to 1600 μg/mL.

Statistics

All comparisons were done with GraphPad Prism 8 software (GraphPad Software, La Jolla, CA, RRID:SCR_002798). A p value of equal or less than 0.05 was considered significant. Detailed statistics for each panel can be found on the Tables and Figures legends. To determine if any observed alleles were associated with the development of antibody-mediated rejection we compared the number of mutated and wild type alleles and patients harboring the mutations in rejecting individuals and in controls samples using Fisher's exact test. Chi-Square test as used to verify if there was a relationship between the *Tnfrsf13b* genotype and early (up to 3 weeks) cardiac allograft rejection, or skin graft rejection (2 weeks).

Study Approval

Informed consent was obtained from all human participants prior to inclusion in the study. Research was approved by the Institutional Review Board of the University of Michigan Medical School. Mice were maintained under specific pathogen-free conditions and all the experiments were performed in accordance with the approved animal protocols and the regulations of University of Michigan Committee on the Use and Care of Animals.

Author contributions: Conceptualization, M.C. and J.L.P.; Methodology, M.G.M.B., M.C. and J.L.P.; Experimental, M.G.M.B., A.R.L., D.H., H.L., Y.Z., B.F., J.B., and E.F; Writing – Original

Draft, M.G.M.B. & M.C.; Writing – Review & Editing, M.G.M.B., E.F., M.S., R.J.B., R.S.G., A.S., E.T.L.P., J.L.P., and M.C.; Funding Acquisition, M.G.M.B., M.C., J.L.P., and A.S.; Resources, M.G.M.B., M.C., J.L.P and E.F.; Supervision, M.G.M.B., M.C. and J.L.P.

Acknowledgments: The microarray analysis was performed by the Advanced Genomics Core at the University of Michigan. **Funding**: This work was supported by the NIH (AI117561, AI122369 and AI 51588 01) to M.C. and J.L.P.; EB 022033, to M.C. and A.S.; by the Department of Surgery at the University of Michigan, the Michigan Genomics Initiative, by two grants from the Michigan Institute for Clinical and Health Research (to M.C. and to M.G.M.B.) and by a grant from the American Society of Transplantation Research Network (to M.G.M.B.).

References:

1. Loeb L. Ueber Entstehung eines Sarkoms nach Transplantation eines Adenocarcinoms einer japanischen Maus. *Zeitschrift für Krebsforschung.* 1908;7(1):34.
2. Medawar PB. The immunology of transplantation. *Harvey Lect.* 1956(Series 52):144-76.
3. Gorer PA. The genetic and antigenic basis of tumour transplantation. *The Journal of Pathology and Bacteriology.* 1937;44(3):691-7.
4. Gorer PA. Studies on the genetic and antigenic basis of tumour transplantation Linkage between a histocompatibility gene and 'fused' in mice. *Proceedings of the Royal Society B.* 1948;135(881):499-505.
5. Auchincloss H, Jr., Lee R, Shea S, Markowitz JS, Grusby MJ, and Glimcher LH. The role of "indirect" recognition in initiating rejection of skin grafts from major histocompatibility complex class II-deficient mice. *Proc Natl Acad Sci U S A.* 1993;90(8):3373-7.
6. Felix NJ, Brickey WJ, Griffiths R, Zhang J, Van Kaer L, Coffman T, et al. H2-DMalpha(-/-) mice show the importance of major histocompatibility complex-bound peptide in cardiac allograft rejection. *J Exp Med.* 2000;192(1):31-40.
7. Pedergnana V, Syx L, Cobat A, Guergnon J, Brice P, Ferme C, et al. Combined linkage and association studies show that HLA class II variants control levels of antibodies against Epstein-Barr virus antigens. *PloS one.* 2014;9(7):e102501.
8. Paun A, Yau C, Meshkibaf S, Daigneault MC, Marandi L, Mortin-Toth S, et al. Association of HLA-dependent islet autoimmunity with systemic antibody responses to intestinal commensal bacteria in children. *Sci Immunol.* 2019;4(32).

9. Tsuji S, Stein L, Kamada N, Nunez G, Bram R, Vallance BA, et al. TACI deficiency enhances antibody avidity and clearance of an intestinal pathogen. *J Clin Invest.* 2014;124(11):4857-66.
10. Cascalho M, and Platt JL. TNFRSF13B Diversification Fueled by B Cell Responses to Environmental Challenges-A Hypothesis. *Front Immunol.* 2021;12:634544.
11. Zerbino DR, Achuthan P, Akanni W, Amode MR, Barrell D, Bhai J, et al. Ensembl 2018. *Nucleic Acids Res.* 2018;46(D1):D754-D61.
12. Siewert KM, and Voight BF. Detecting Long-Term Balancing Selection Using Allele Frequency Correlation. *Mol Biol Evol.* 2017;34(11):2996-3005.
13. Lek M, Karczewski KJ, Minikel EV, Samocha KE, Banks E, Fennell T, et al. Analysis of protein-coding genetic variation in 60,706 humans. *Nature.* 2016;536(7616):285-91.
14. Quintana-Murci L. Human Immunology through the Lens of Evolutionary Genetics. *Cell.* 2019;177(1):184-99.
15. Mantchev GT, Cortesao CS, Rebrovich M, Cascalho M, and Bram RJ. TACI is required for efficient plasma cell differentiation in response to T-independent type 2 antigens. *J Immunol.* 2007;179(4):2282-8.
16. Romberg N, Chamberlain N, Saadoun D, Gentile M, Kinnunen T, Ng YS, et al. CVID-associated TACI mutations affect autoreactive B cell selection and activation. *J Clin Invest.* 2013;123(10):4283-93.
17. Loupy A, Aubert O, Orandi BJ, Naesens M, Bouatou Y, Raynaud M, et al. Prediction system for risk of allograft loss in patients receiving kidney transplants: international derivation and validation study. *BMJ.* 2019;366:l4923.
18. Huang Y, Ramon D, Luan FL, Sung R, and Samaniego M. Incidences of preformed and de novo donor-specific HLA antibodies and their clinicohistological correlates in the early course of kidney transplantation. *Clin Transpl.* 2012:247-56.
19. Bartel G, Wahrmann M, Exner M, Regele H, Huttary N, Schillinger M, et al. In vitro detection of C4d-fixing HLA alloantibodies: associations with capillary C4d deposition in kidney allografts. *Am J Transplant.* 2008;8(1):41-9.
20. Yell M, Muth BL, Kaufman DB, Djamali A, and Ellis TM. C1q Binding Activity of De Novo Donor-specific HLA Antibodies in Renal Transplant Recipients With and Without Antibody-mediated Rejection. *Transplantation.* 2015;99(6):1151-5.
21. Castigli E, Wilson SA, Garibyan L, Rachid R, Bonilla F, Schneider L, et al. TACI is mutant in common variable immunodeficiency and IgA deficiency. *Nat Genet.* 2005;37(8):829-34.
22. Kumar P, Henikoff S, and Ng PC. Predicting the effects of coding non-synonymous variants on protein function using the SIFT algorithm. *Nat Protoc.* 2009;4(7):1073-81.
23. Adzhubei I, Jordan DM, and Sunyaev SR. Predicting functional effect of human missense mutations using PolyPhen-2. *Curr Protoc Hum Genet.* 2013;Chapter 7:Unit7 20.
24. Rentzsch P, Witten D, Cooper GM, Shendure J, and Kircher M. CADD: predicting the deleteriousness of variants throughout the human genome. *Nucleic Acids Res.* 2019;47(D1):D886-D94.
25. Ioannidis NM, Rothstein JH, Pejaver V, Middha S, McDonnell SK, Baheti S, et al. REVEL: An Ensemble Method for Predicting the Pathogenicity of Rare Missense Variants. *American journal of human genetics.* 2016;99(4):877-85.
26. Liu X, Wu C, Li C, and Boerwinkle E. dbNSFP v3.0: A One-Stop Database of Functional Predictions and Annotations for Human Nonsynonymous and Splice-Site SNVs. *Hum Mutat.* 2016;37(3):235-41.
27. Nozaki T, Amano H, Bickerstaff A, Orosz CG, Novick AC, Tanabe K, et al. Antibody-mediated rejection of cardiac allografts in CCR5-deficient recipients. *J Immunol.* 2007;179(8):5238-45.
28. Tsuji S, Cortesão C, Bram R, Platt JL, and Cascalho M. TACI deficiency impairs sustained Blimp-1 expression in B cells decreasing long-lived plasma cells in the bone marrow. *Blood.* 2011;118(22):5832-9.

29. Tsuji S, Cortesao C, Bram RJ, Platt JL, and Cascalho M. TACI deficiency impairs sustained Blimp-1 expression in B cells decreasing long-lived plasma cells in the bone marrow. *Blood.* 2011;118(22):5832-9.
30. Newell KA, Asare A, Kirk AD, Gisler TD, Bourcier K, Suthanthiran M, et al. Identification of a B cell signature associated with renal transplant tolerance in humans. *Journal of Clinical Investigation.* 2010;120(6):1836-47.
31. Platt JL. Antibodies in transplantation. *Discov Med.* 2010;10(51):125-33.
32. Rieben R, Roos A, Muizert Y, Tinguely C, Gerritsen AF, and Daha MR. Immunoglobulin M-enriched human intravenous immunoglobulin prevents complement activation in vitro and in vivo in a rat model of acute inflammation. *Blood.* 1999;93(3):942-51.
33. Lobo PI. Role of Natural Autoantibodies and Natural IgM Anti-Leucocyte Autoantibodies in Health and Disease. *Front Immunol.* 2016;7:198.
34. Lobo PI, Bajwa A, Schlegel KH, Vengal J, Lee SJ, Huang L, et al. Natural IgM anti-leukocyte autoantibodies attenuate excess inflammation mediated by innate and adaptive immune mechanisms involving Th-17. *J Immunol.* 2012;188(4):1675-85.
35. Miletic VD, Hester CG, and Frank MM. Regulation of complement activity by immunoglobulin. I. Effect of immunoglobulin isotype on C4 uptake on antibody-sensitized sheep erythrocytes and solid phase immune complexes. *J Immunol.* 1996;156(2):749-57.
36. Frank MM, Miletic VD, and Jiang H. Immunoglobulin in the control of complement action. *Immunol Res.* 2000;22(2-3):137-46.
37. Cascalho M, Ma A, Lee S, Masat L, and Wabl M. A quasi-monoclonal mouse. *Science.* 1996;272(5268):1649-52.
38. Cascalho M, Wong J, and Wabl M. VH gene replacement in hyperselected B cells of the quasimonoclonal mouse. *Journal of immunology.* 1997;159(12):5795-801.
39. Jabara HH, Lee JJ, Janssen E, Ullas S, Liadaki K, Garibyan L, et al. Heterozygosity for transmembrane activator and calcium modulator ligand interactor A144E causes haploinsufficiency and pneumococcal susceptibility in mice. *J Allergy Clin Immunol.* 2017;139(4):1293-301 e4.
40. Ballow M. Primary immunodeficiency disorders: antibody deficiency. *J Allergy Clin Immunol.* 2002;109(4):581-91.
41. Carsetti R, Rosado MM, Donnanno S, Guazzi V, Soresina A, Meini A, et al. The loss of IgM memory B cells correlates with clinical disease in common variable immunodeficiency. *J Allergy Clin Immunol.* 2005;115(2):412-7.
42. Salzer U, Chapel HM, Webster AD, Pan-Hammarstrom Q, Schmitt-Graeff A, Schlesier M, et al. Mutations in TNFRSF13B encoding TACI are associated with common variable immunodeficiency in humans. *Nat Genet.* 2005;37(8):820-8.
43. von Bulow GU, and Bram RJ. NF-AT activation induced by a CAML-interacting member of the tumor necrosis factor receptor superfamily. *Science.* 1997;278(5335):138-41.
44. Ozcan E, Garibyan L, Lee JJ, Bram RJ, Lam KP, and Geha RS. Transmembrane activator, calcium modulator, and cyclophilin ligand interactor drives plasma cell differentiation in LPS-activated B cells. *J Allergy Clin Immunol.* 2009;123(6):1277-86 e5.
45. Castigli E, Wilson SA, Scott S, Dedeoglu F, Xu S, Lam KP, et al. TACI and BAFF-R mediate isotype switching in B cells. *J Exp Med.* 2005;201(1):35-9.
46. Lee JJ, Rauter I, Garibyan L, Ozcan E, Sannikova T, Dillon SR, et al. The murine equivalent of the A181E TACI mutation associated with common variable immunodeficiency severely impairs B-cell function. *Blood.* 2009;114(11):2254-62.
47. Sintes J, Gentile M, Zhang S, Garcia-Carmona Y, Magri G, Cassis L, et al. mTOR intersects antibody-inducing signals from TACI in marginal zone B cells. *Nat Commun.* 2017;8(1):1462.

48. Lescure FX, Bouadma L, Nguyen D, Parisey M, Wicky PH, Behillil S, et al. Clinical and virological data of the first cases of COVID-19 in Europe: a case series. *Lancet Infect Dis.* 2020.
49. Chen G, Wu D, Guo W, Cao Y, Huang D, Wang H, et al. Clinical and immunological features of severe and moderate coronavirus disease 2019. *J Clin Invest.* 2020.
50. Hernandez-Fuentes M, Stapleton CP, Cavalleri GL, Conlon P, Weale ME, Lord GM, et al. The genetic determinants of renal allograft rejection. *Am J Transplant.* 2018;18(8):2100-1.
51. Massart A, Ghisdal L, Viklicky O, Naesens M, Abramowicz D, and Abramowicz M. Reply to Hernandez et al. - GWAS of acute renal graft rejection. *Am J Transplant.* 2018;18(8):2098-9.
52. Oetting WS, Schladt DP, Leduc RE, Jacobson PA, Guan W, Matas AJ, et al. Validation of single nucleotide polymorphisms associated with acute rejection in kidney transplant recipients using a large multi-center cohort. *Transpl Int.* 2011;24(12):1231-8.
53. Sis B, Bagnasco SM, Cornell LD, Randhawa P, Haas M, Lategan B, et al. Isolated endarteritis and kidney transplant survival: a multicenter collaborative study. *J Am Soc Nephrol.* 2015;26(5):1216-27.
54. von Bulow GU, van Deursen JM, and Bram RJ. Regulation of the T-independent humoral response by TACI. *Immunity.* 2001;14(5):573-82.
55. Irizarry RA, Hobbs B, Collin F, Beazer-Barclay YD, Antonellis KJ, Scherf U, et al. Exploration, normalization, and summaries of high density oligonucleotide array probe level data. *Biostatistics.* 2003;4(2):249-64.
56. Smyth GK. Linear models and empirical bayes methods for assessing differential expression in microarray experiments. *Stat Appl Genet Mol Biol.* 2004;3:Article3.
57. Ritchie ME, Diyagama D, Neilson J, van Laar R, Dobrovic A, Holloway A, et al. Empirical array quality weights in the analysis of microarray data. *BMC bioinformatics.* 2006;7:261.
58. Benjamini Y, and Hochberg Y. Controlling the False Discovery Rate: A Practical and Powerful Approach to Multiple Testing. *Journal of the Royal Statistical Society Series B (Methodological).* 1995;57(1):289-300.
59. Singh H, Henry KA, Wu SS, Chruscinski A, Utz PJ, and Scott JK. Reactivity profiles of broadly neutralizing anti-HIV-1 antibodies are distinct from those of pathogenic autoantibodies. *Aids.* 2011;25(10):1247-57.

Figure Legends

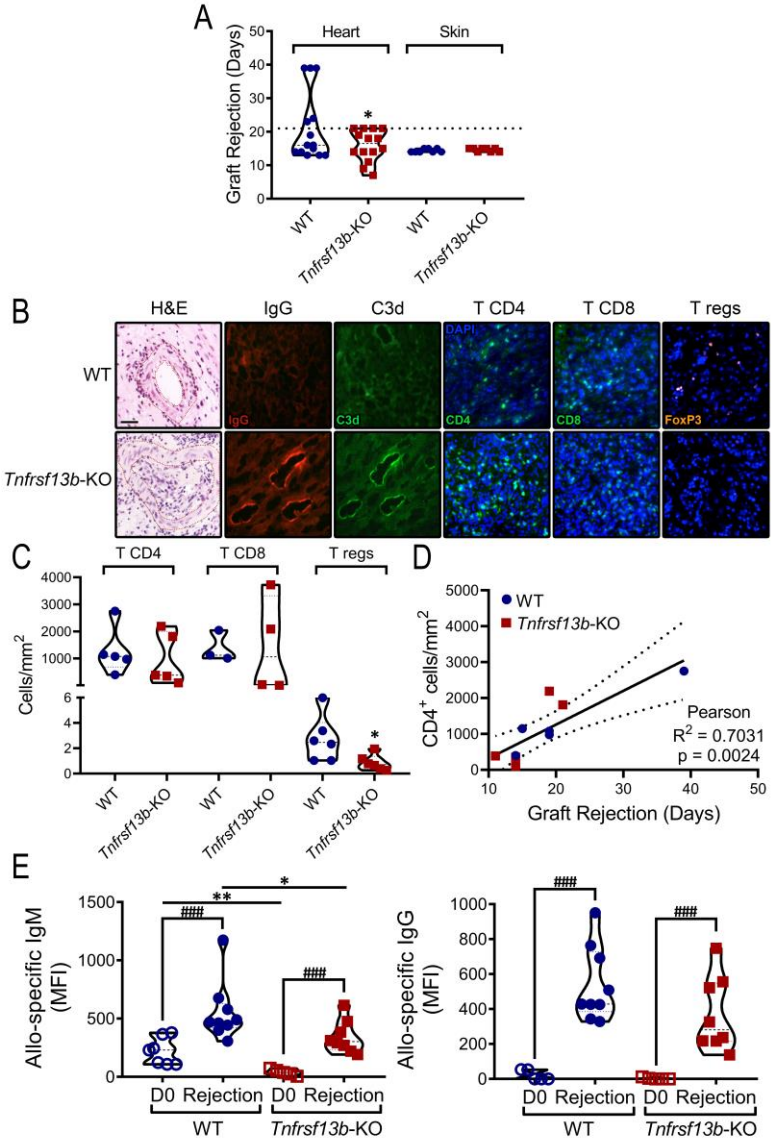

Figure 1. ***Tnfrsf13b*** **deficiency evokes antibody responses to allografts and accelerates rejection of heart allografts.** Hearts (transplanted heterotopically into the abdomen) and skin from CB6F1 mice (C57BL/6-BALB/c F1, H-$2^{b/d}$ haplotype) were transplanted into C57BL/6 (H-$2^{b/b}$ haplotype) WT and *Tnfrsf13b*-KO mice and allograft survival was evaluated daily until rejection. **(A)** Graph represents the Mean ± SEM of the number of days elapsed until allograft rejection (n=14). See also Table 2. **(B)** Hematoxylin-Eosin (H&E) staining, anti-IgG, anti-C3d, anti-CD4, anti-CD8 and anti-Foxp3 (to detect T regulatory cells, Treg) immunostainings. Images are representative of a mouse of each group with viable heart excision at day 14 (H&E, C3d and IgG staining) or at rejection in day 19 (CD4, CD8 and Foxp3 staining). See also Figure S1. Bar: 25 µm. **(C)** Graph depicts the number of $CD4^+$, $CD8^+$ of $Foxp3^+$ (Tregs) T cells per mm^2 in sections counted in 5 non-overlapping fields obtained from grafts at rejection. **(D)** Graph represents the relationship between number of $CD4^+$ T cells in graft sections and length of transplantation. Statistical analysis (Pearson correlation, p=0.0024) indicates that the number of CD4+ T cells/ mm^2 increases with time from transplantation. **(E)** Sera of recipient mice were collected before transplantation (day 0, D0) and at time of rejection and allo-specific IgM and IgG were analyzed by flow cytometry. Graphs are representative of Mean ± SEM of 7-9 mice per group. Unpaired T test **(A, C, E)** or Mann-Whitney test **(E)**: * $p \leq 0.05$, ** $p \leq 0.01$ in relation to WT control; ### $p \leq 0.001$ in relation to day 0 (D0).

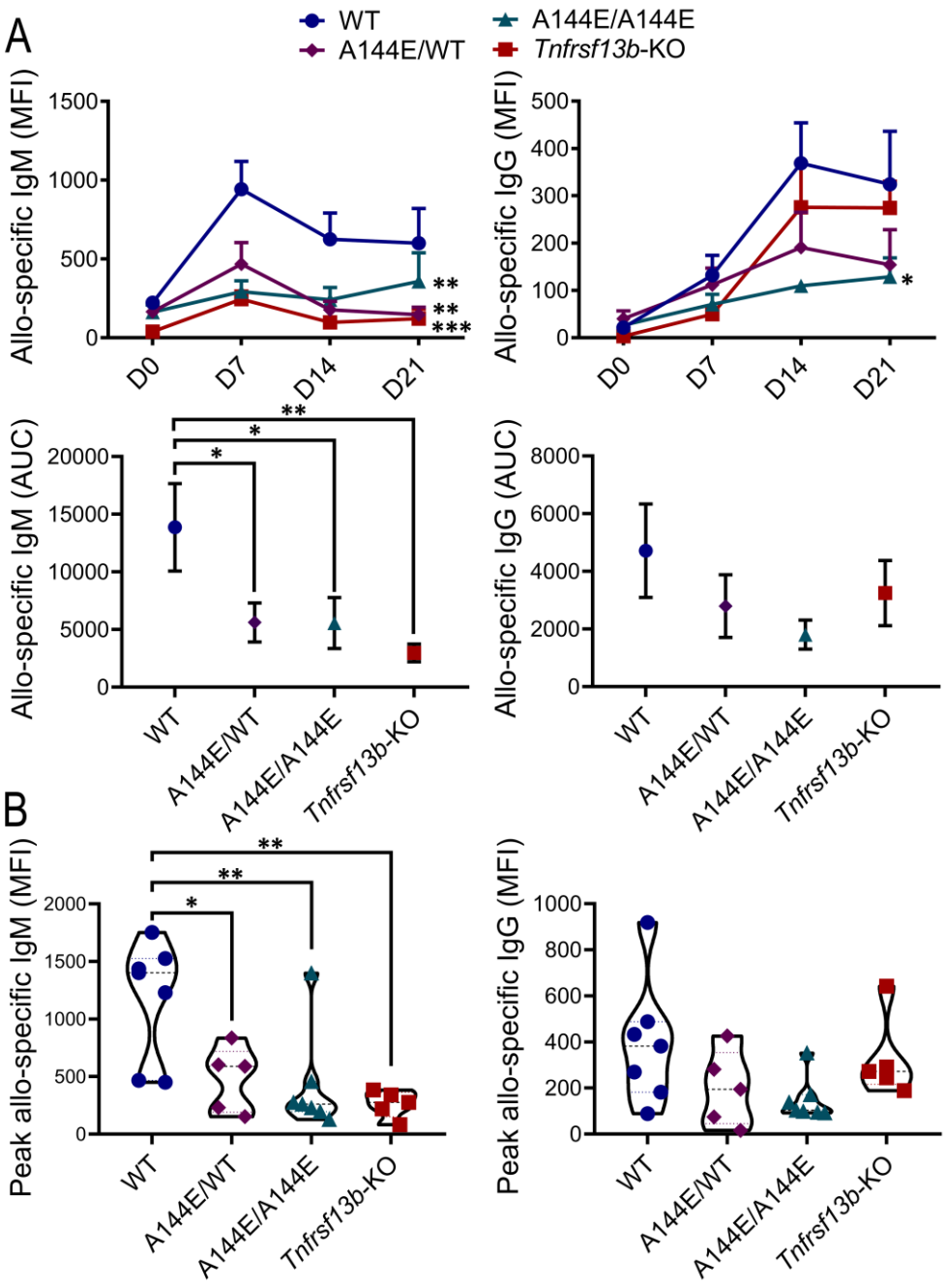

Figure 2. *Tnfrsf13b* genotype determines IgM responses to allo-antigens. Mice were immunized by intraperitoneal injection with 5 x 10^7 BALB/c splenocytes and thymocytes. Blood was collected weekly and levels of allo-specific antibodies that bound BALB/c thymocytes were measured by flow cytometry pre- (day 0, D0) and post-immunization with allogeneic cells (days 7-21, D7, D14, D21). **(A)** Kinetics of allo-specific IgM and IgG response were analyzed by flow cytometry. Curves were compared by Two-Way RM ANOVA followed by Dunnett's multiple comparisons test. Area under the curve (AUC) was analyzed using the AUC function on GraphPad Prism 8. AUCs were compared using Brown-Forsythe ANOVA test followed by Dunnett's multiple comparisons tests and by unpaired T tests with Welch's correction (shown). **(B)** The peak concentrations of allo-specific IgM and IgG in the blood are shown. Graphs are representative of Mean ± SEM of 5-7 mice per group. Analysis was by One-Way ANOVA followed by Dunnett's multiple comparisons tests. * $p \leq 0.05$; ** $p \leq 0.01$; *** $p \leq 0.001$ in relation to WT control.

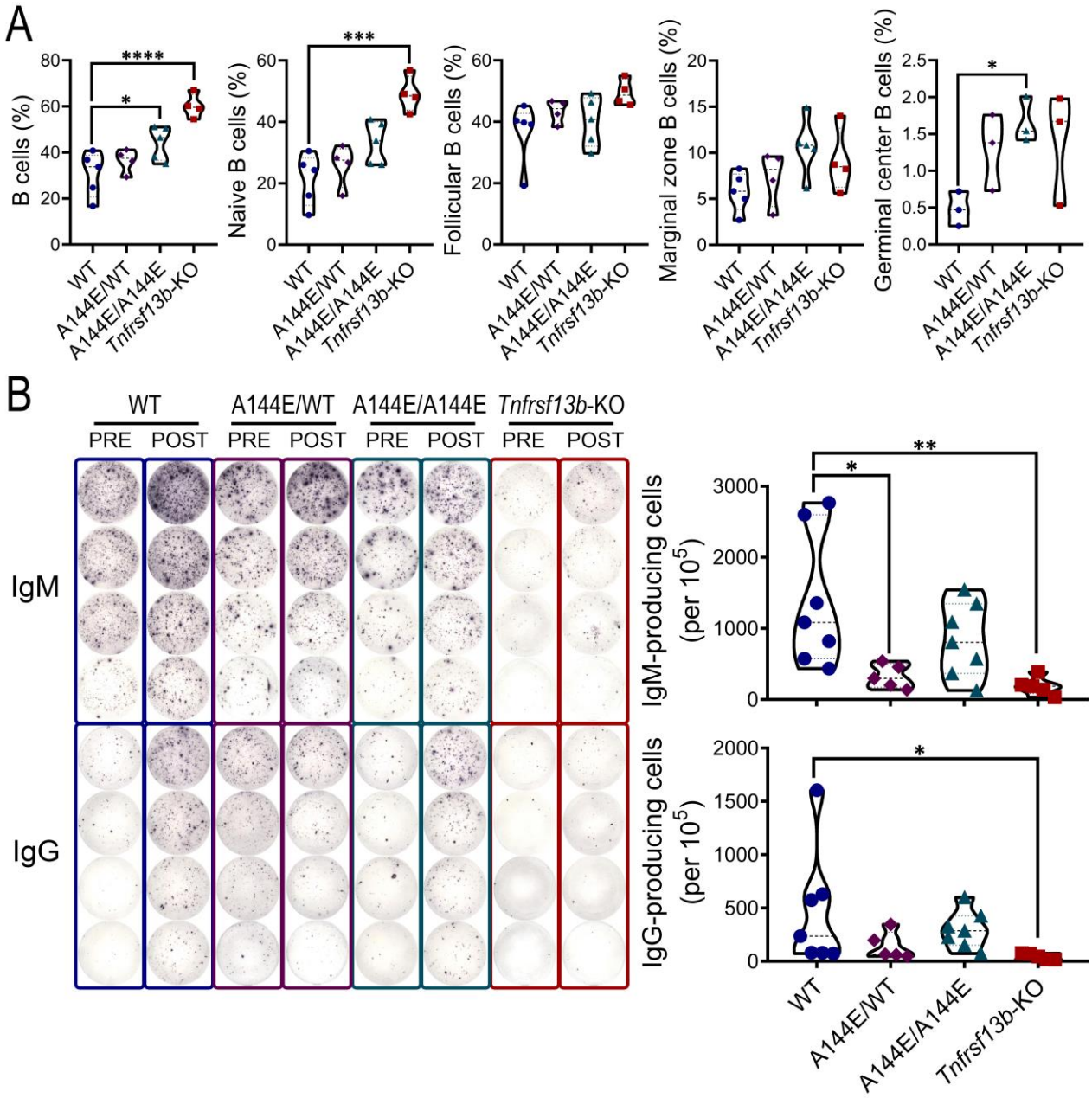

Figure 3. *Tnfrsf13b* deficiency impairs the differentiation of antibody-secreting cells in response to allo-antigens. Mice were immunized by intraperitoneal injection with 5 x 10^7 BALB/c splenocytes and thymocytes, spleens were harvested 10-21 days post-immunization. **(A)** Splenic percentages of live lymphocytes with phenotypes of B cells ($CD19^+$), naive B cells ($CD19^+$ IgD^+) and percentages of $CD19^+$ B cells that were marginal zone ($CD19^+$ $CD21^{high}$ $CD23^-$), follicular ($CD19^+$ $CD21^+$ $CD23^+$) (at day 21) and germinal center ($CD19^+$ $CD95^+$ $GL7^+$) B cells in the spleen (at day 10 post allo-immunization). **(B)** ELISPOT of IgM- and IgG-secreting cells pre- (day 0) and 21 days post-allo-immunization. Graphs are representative of Mean ± SEM of 3-7 mice per group 21 days post-allo-immunization. One-Way ANOVA or Brown-Forsythe and Welch's ANOVA test with Dunnett's multiple comparisons test: * $p \leq 0.05$; ** $p \leq 0.01$; *** $p \leq 0.001$; **** $p \leq 0.0001$ in relation to the WT control.

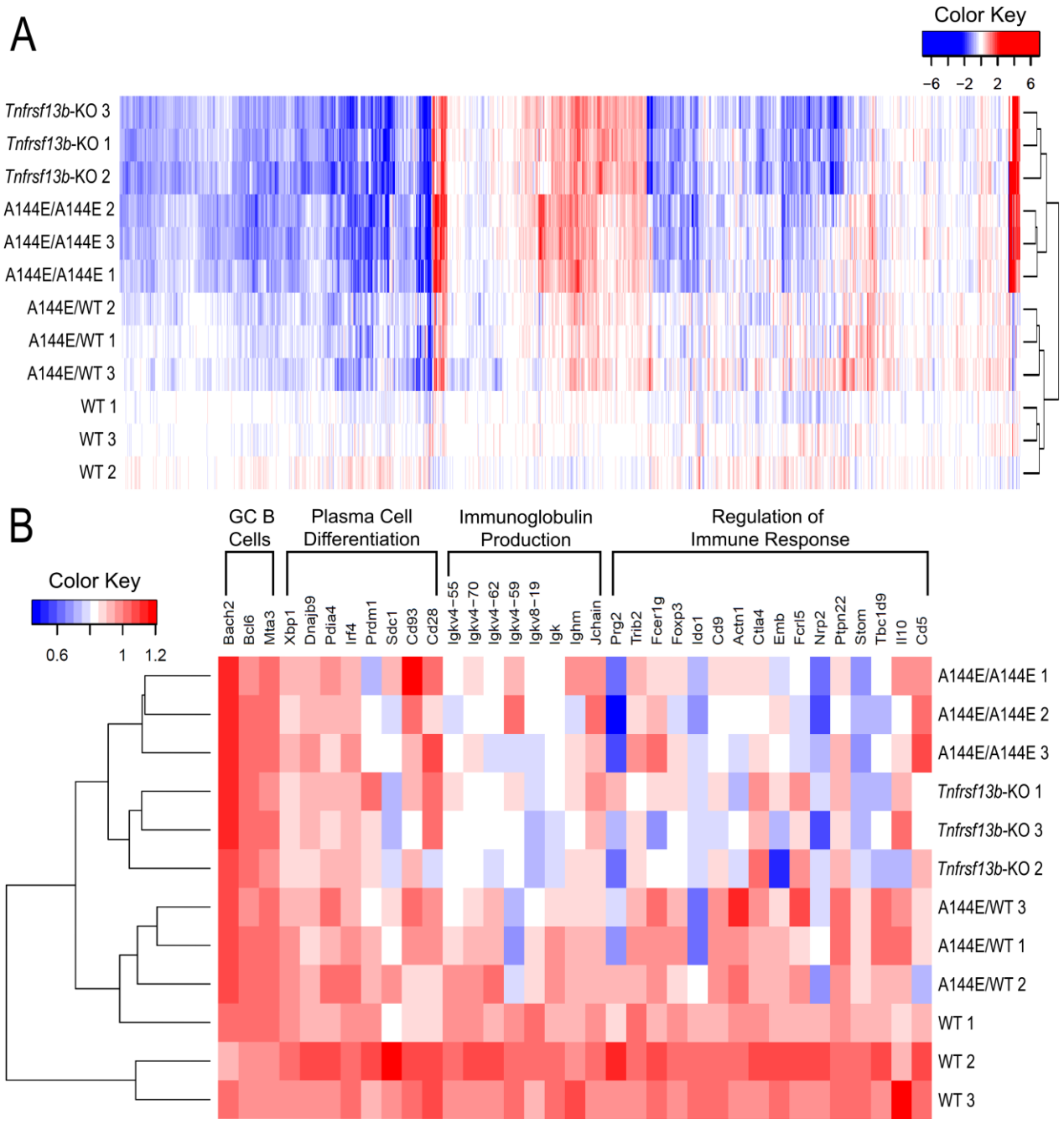

Figure 4. Microarray analysis of germinal center B cells of allo-immunized *Tnfrsf13b*-mutant mice. Mice with different *Tnfrsf13b* genotypes were immunized by intraperitoneal injection with 5 x 10^7 BALB/c splenocytes and thymocytes. Spleens from immunized mice were collected 10 days later and live $CD19^+$ $CD95^+$ $GL7^+$ germinal center (GC) B cells were sorted, and gene expression was assessed by microarray (see also Figure S4 and Table S2). **(A)** Heat map representing expression of genes found to be either significantly upregulated (red) or downregulated (blue) in the different *Tnfrsf13b* genotypes compared to WT. Each row represents one mouse (n=3). **(B)** Expression of signature genes of germinal center (GC) B cells, plasma cells, and immunoglobulin production and regulation of immune response pathways found to be either upregulated (red) or downregulated (blue) by *Tnfrsf13b* deficiency (n=3).

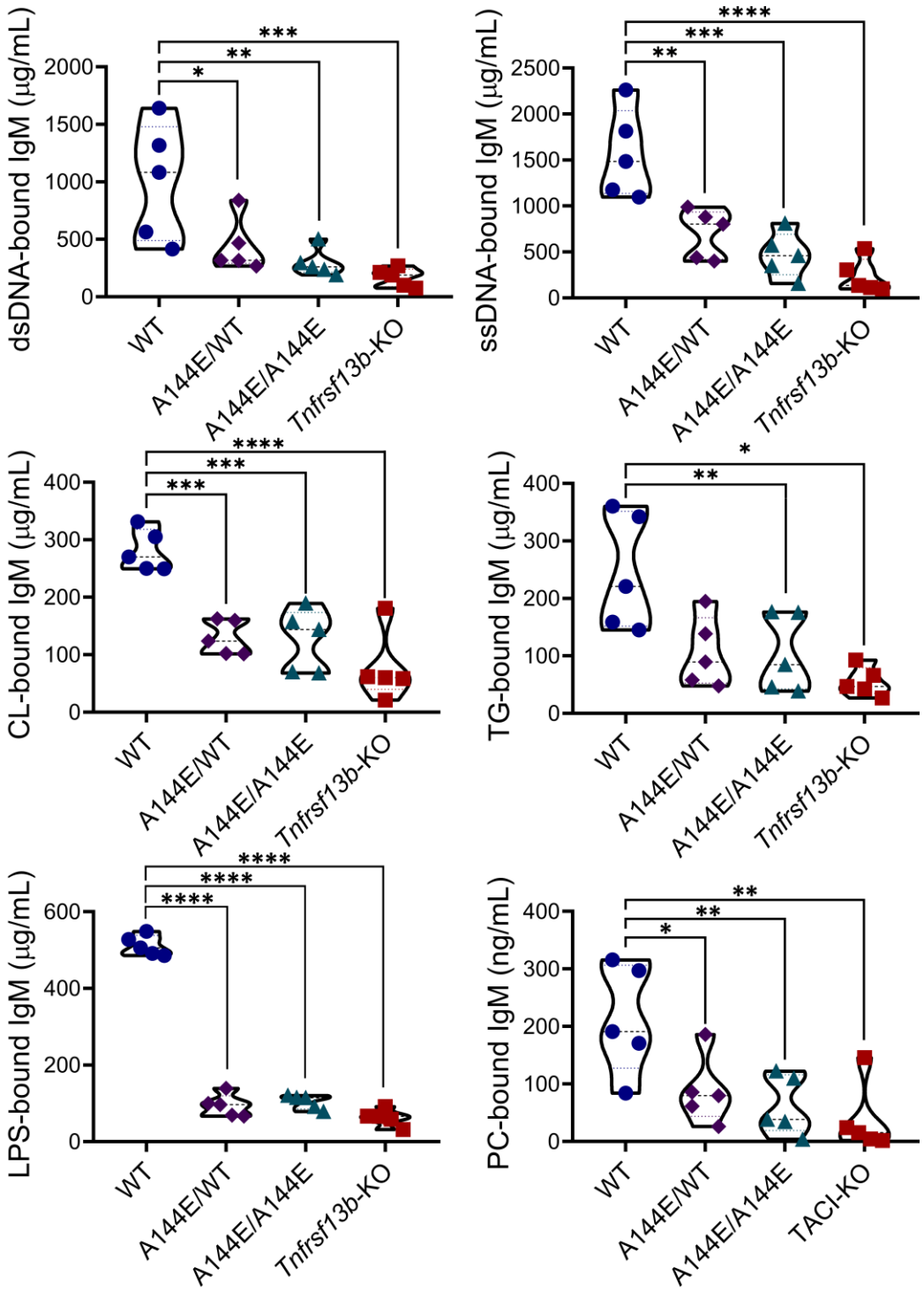

Figure 5. ***Tnfrsf13b*** **controls the production of natural IgM.** Mice were immunized via intraperitoneal injection with 5 x 10^7 BALB/c splenocytes and thymocytes and serum was collected weekly. Serum levels of natural IgM reactive to double-stranded DNA (dsDNA), single-stranded DNA (ssDNA), cardiolipin (CL), thyroglobulin (TG), lipopolysaccharide (LPS) and phosphocholine (PC) 14 days after immunization with allogeneic cells. Graphs are representative of Mean ± SEM of 5 mice per group. One-way ANOVA with Dunnett's multiple comparison test: * $p \leq 0.05$; ** $p \leq 0.01$; *** $p \leq 0.001$; **** $p \leq 0.0001$ in relation to WT control.

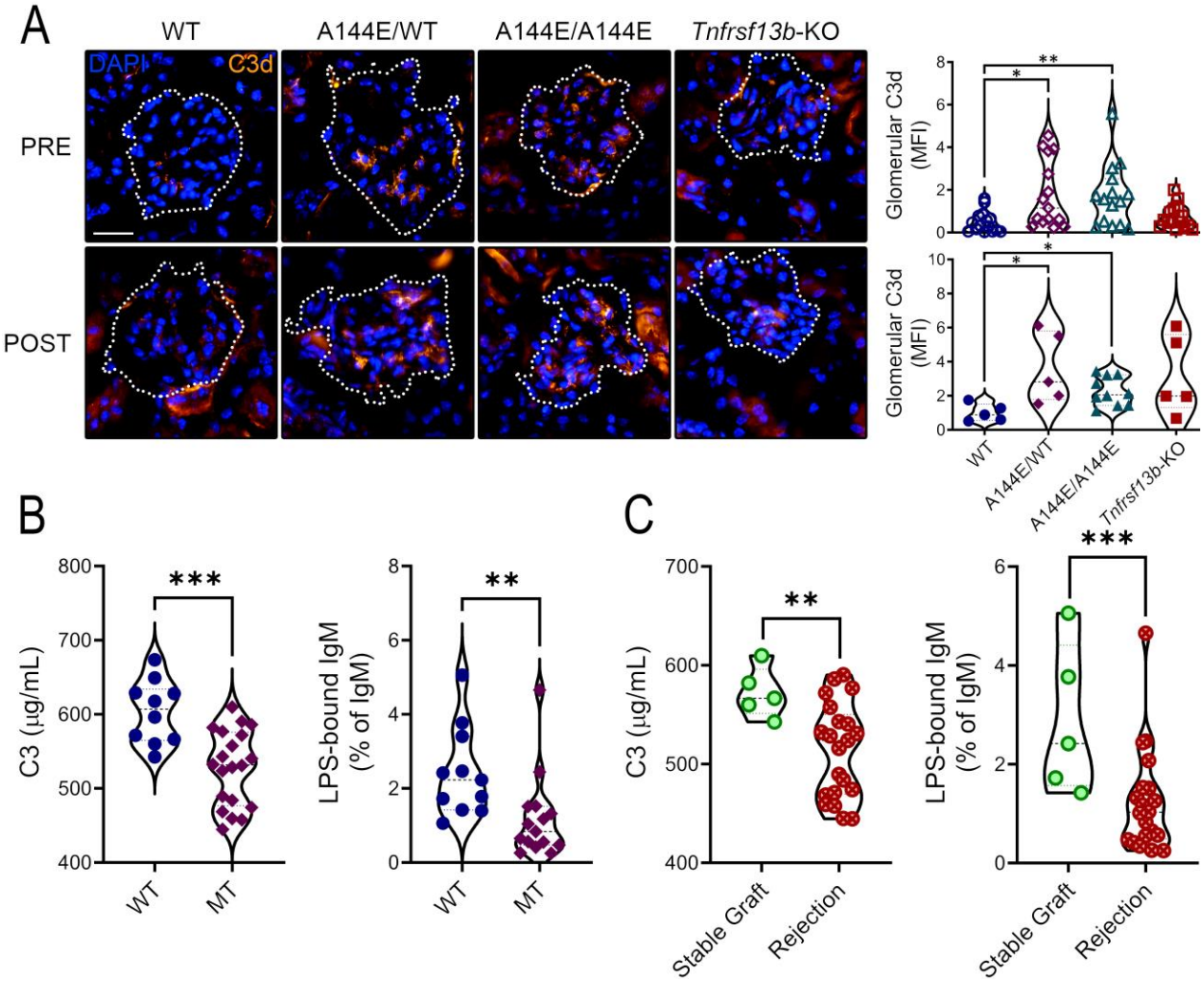

Figure 6. ***Tnfrsf13b*** **controls immune and inflammatory injury.** **(A)** Native kidneys were harvested from naïve mice (pre) or mice immunized with 5 x 10^7 BALB/c splenocytes and thymocytes by intraperitoneal injection (post). Glomerular C3d deposits were identified with anti-mouse C3d immunostaining in frozen native kidney sections pre- or 8 days post-allogeneic stimulation. Graphs show Mean ± SEM calculated from analysis of 5-7 fields with 3 or more glomeruli per mouse per group. Open shapes represent data from naive mice (pre) and filled shapes represent data of mice 8 days of post-immunization (post). **(B and C)** Blood samples were collected from patients that underwent kidney transplantation after transplantation. The patients' *TNFRSF13B* gene exons were sequenced, and the patients were classified according to the absence or presence of missense mutations, as *TNFRSF13B* WT or mutant (MT), respectively, independently of transplantation outcome **(B)** or according with the transplant outcome **(C)**. The concentrations of natural LPS-binding IgM and C3 in sera were measured by ELISA. Graphs show Mean ± SEM of 8-14 individuals per group. Kruskal-Wallis with Dunn's multiple comparison test **(A)**, Mann-Whitney test **(B, C)**: * $p \leq 0.05$; ** $p \leq 0.01$; *** $p \leq 0.001$; in relation to WT control.

Supplementary Figure Legends:

Figure S1. Anti-IgM, IgG and C3d immunostainings in transplanted hearts 14 days after transplantation. Hearts from CB6F1 mice (C57BL/6-BALB/c F1, H-$2^{b/d}$ haplotype) were transplanted heterotopically into the abdomen of C57BL/6 (H-$2^{b/b}$ haplotype) WT and *Tnfrsf13b*-KO. Deposition of IgM, IgG and C3d was evaluated by immunofluorescence. **(A)** Anti-IgM immunostaining of sections obtained from cardiac allografts excised at day 14. Images are representative of a mouse of each group. **(B)** Anti-IgG and anti-C3d immunostainings of sections obtained from cardiac allografts at rejection. Images are representative of two mice of each group. See also Figure 1. Bars: 40 µm.

Figure S2. Anti-IgM, IgG and C3d immunostainings of sections of native hearts obtained at rejection of cardiac allografts. Hearts from CB6F1 mice (C57BL/6-BALB/c F1, H-$2^{b/d}$ haplotype) were transplanted heterotopically into the abdomen of C57BL/6 (H-$2^{b/b}$ haplotype) WT and *Tnfrsf13b*-KO. Both transplanted and native hearts were retrieved at rejection. Deposition of IgM, IgG and C3d into the native heart was evaluated by immunofluorescence. Images are representative of a mouse of each group. Bar: 40 µm.

Figure S3. Splenic B cell populations in *Tnfrsf13b*-mutant mice. Spleens from naïve mice with different *Tnfrsf13b* genotypes were harvested. Splenic percentages of live lymphocytes with phenotypes of B cells ($CD19^+$), naive B cells ($CD19^+$ IgD^+) and percentages of $CD19^+$ B cells that were marginal zone ($CD19^+$ $CD21^{high}$ $CD23^-$), follicular ($CD19^+$ $CD21^+$ $CD23^+$) and germinal center ($CD19^+$ $CD95^+$ $GL7^+$) B cells in the spleen. Graphs are representative of Mean ± SEM of 3 naïve mice per group. Mann-Whitney test: * $p \leq 0.05$ in relation to the WT control.

Figure S4. Germinal center B cells sorting and microarray quality analysis. Mice were immunized by intraperitoneal injection with 5 x 10^7 allogenic splenocytes and thymocytes. Spleens were collected after 10 days, germinal center (GC) B cells were sorted, RNA was extracted, and gene expression was analyzed by microarray. **(A)** Singlet viable lymphocytes that were $CD19^+$ (B cells) were further analyzed for the expression of GL7 and FAS (CD95). B cells with a GC phenotype ($CD19^+$ $CD95^+$ $GL7^+$) were sorted (green) for RNA microarray analysis. **(B)** Probe densities in each microarray chip analyzed (n = 3). **(C)** Box plot shows the standard errors for each array calculated after fitting a probe-level model. **(D)** Distribution of analyzed samples in the first two principal components, responsible for 31% of the variation in the principal component analysis. Colored ellipses represent clustered samples by genotype. Sample numbers: 1-3 WT, 4-6 *Tnfrsf13b*-KO, 7-9 A144E/WT, 10-12 A144E/A144E.

Figure S5. *Tnfrsf13b* deficiency evokes decreased IgM and increased IgG responses to allografts and allo-immunization. (A and B) Hearts from CB6F1 mice (C57BL/6-BALB/c F1, H-$2^{b/d}$ haplotype) were transplanted heterotopically into the abdomen of C57BL/6 (H-$2^{b/b}$ haplotype) WT and *Tnfrsf13b*-KO mice and sera of recipient mice were collected at time of transplant and at rejection. **(A)** Graphs represent the Mean ± SEM of concentrations of total IgM and IgG before transplantation (Day 0) and at rejection of 5-7 mice per group. **(B)** Paired analysis of immunoglobulin concentrations before transplantation (Day 0, green) and at rejection (red). **(C)** Mice were immunized via intraperitoneal injection with 5 x 10^7 BALB/c splenocytes and thymocytes, blood was collected weekly for 21 days. The concentrations of total IgM and IgG at the peak of the response post-immunization with allogeneic cells. Graphs are representative of Mean ± SEM of 5-7 mice per group. Unpaired **(A, B),** paired T test **(B),** Mann-Whitney test **(B, C),** One-Way ANOVA with Dunnett's multiple comparison test or Kruskal-Wallis with Dunn's multiple comparison test **(C)**: * $p \leq 0.05$; ** $p \leq 0.01$; *** $p \leq 0.001$; **** $p \leq 0.0001$ in relation to WT control; # $p \leq 0.05$; ### $p \leq 0.001$ in relation to day 0 (D0).

Figure S6. *Tnfrsf13b* protects native kidneys from immune and inflammatory injury. (A and B) Native kidneys were harvested from naïve mice (pre) or mice immunized via intraperitoneal injection with 5 x 10^7 BALB/c splenocytes and thymocytes (post). Glomerular IgM **(A)** and IgG **(B)** deposits were examined with anti-mouse IgM or IgG immunostaining of frozen native kidney sections pre- or 8 days post-allogeneic stimulation. Graphs show Mean ± SEM calculated from analysis of 5-7 fields with 3 or more glomeruli per mouse per group. Open shapes represent data from naive mice (pre) and filled shapes represent data of mice 8 days of post-immunization (post). One-Way ANOVA with Dunnett's multiple comparison test or Kruskal-Wallis with Dunn's multiple comparison test: * $p \leq 0.05$; ** $p \leq 0.01$; **** $p \leq 0.0001$ in relation to WT control.

Figure S7. C3d and IgG deposition in native kidneys of natural antibody-deficient mice. Native kidneys were harvested from naive Quasi-Monoclonal (QM) mice *Tnfrsf13b* proficient or deficient. Quasi-Monoclonal mice produce

only 4-hydroxy-3-nitrophenyl-acetyl (NP)-specific IgM and lack natural IgM. Glomerular C3d deposits **(A)** or IgG **(B)** were identified with anti-mouse C3d or goat anti-mouse IgG on frozen sections obtained from native kidneys. Figures show typical sections obtained from two distinct *Tnfrsf13b* proficient (left) or deficient (right) Quasi-Monoclonal mice, representative from stainings in 7 different mice of each genetic background. Bar: 25 µm. **(C)** Hearts (transplanted heterotopically into the abdomen) from BALB/c mice H-$2^{d/d}$ haplotype) were transplanted into C57BL/6 (H-$2^{b/b}$ haplotype) WT and QM mice and allograft survival was evaluated daily until rejection. Graph depicts the survival curves showing overlapping rejection kinetics.

Tables

Table 1. *TNFRSF13B* missense mutations in kidney transplant recipients. Missense mutations on exons 3, 4 and 5 reported in kidney transplant recipients that developed antibody-mediated rejection (AMR) or had stable graft function during a period up to 5 years after transplantation. One individual with AMR was a compound heterozygote with two mutations on exon 4, A173T and K188M. Significant differences are denoted in bold.

		AMR			**Stable Graft Function**			**Fisher's Exact Test**
Exon	**Missense Mutation**	**# Alleles**		**Allele Frequency (%)**	**# Alleles**		**Allele Frequency (%)**	**p Value**
		MT	**WT**		**MT**	**WT**		
Exon 3	**C104R**	1	255	0.39	0	238	0.00	0.5182
Exon 4	**A173T**	1	333	0.30	0	230	0.00	0.5922
	A181E	2	332	0.60	0	230	0.00	0.3503
	K188del	1	333	0.30	0	230	0.00	0.5922
	K188M	6	328	1.80	0	230	0.00	**0.0423**
	R189M	1	333	0.30	0	230	0.00	0.5922
	G190R	1	333	0.30	0	230	0.00	0.5922
	S209F	1	333	0.30	0	230	0.00	0.5922
	All Variants on Exon 4	13	321	3.89	0	230	0.00	**0.001**
Exon 5	**P251L**	29	169	14.65	6	198	2.94	**<0.0001**
All Exons	**All Variants**	43	-	18.93	6	-	2.94	**<0.0001**

Abbreviations: AMR, Antibody-mediated rejection; MT, Mutated; WT, Wild type.

Table S1. Predicted impact of *TNFRSF13B* mutations on protein function. Impact of *TNFRSF13B* missense mutations on protein structure and function, according to SIFT, PolyPhen-2, CADD, REVEL, MetaLR and MutationAssessor prediction tools and the ClinVar database.

Table 2. Time of rejection of heart and skin (H-$2^{b/d}$) allografts in C57BL/6 wild type and *Tnfrsf13b*-KO mice (H-$2^{b/b}$). Chi-Square test was performed at the 3 weeks' timepoint for heart and at 2 weeks for skin allografts. Significant differences are noted (bold).

Graft	Strain	n	Rejection Average (Min-Max)	Chi-Square p Value
Heart	**WT**	14	21.21 (13-39)	**0.0136**
	***Tnfrsf13b*-KO**	14	15.93 (7-21)	
Skin	**WT**	8	14.38 (14-15)	0.3173
	***Tnfrsf13b*-KO**	8	14.63 (14-15)	

Abbreviations: WT, Wild type; *Tnfrsf13b*-KO, *Tnfrsf13b* knockout; Min, Minimum; Max, Maximum.

Table S2. Top 500 germinal center B cell genes differentially expressed between wild type and *Tnfrsf13b*-mutant mice 10 days post-allogenic stimulation.